Dear Dr. Tian,

Thank you so much for overseeing the review of our manuscript. We would like to thank the anonymous referee for their positive and constructive review comments.

Thank you very much for reviewing our manuscript. We would like to express our gratitude to the anonymous reviewers for their positive and constructive review comments. The manuscript has greatly benefited from their insightful suggestions. We have made significant changes to the manuscript based on their recommendations and would like to share our responses to their comments below.

Firstly, we acknowledge that there is room for improvement in the RF modelling details, theoretical flaws in the core assumptions, and the lack of field validation of the RFSTM/TSETR method. Therefore, we have addressed these issues by revising the Methods, Results, and Discussion sections, as well as the rest of the paper. Our aim was to enhance the credibility of the method, specifically TRISM LST.

Moreover, in response to the suggestions made by two reviewers, we have added data in NETCDF format as an option and utilized a more general zip compression format. These changes will provide greater flexibility and ease of use for researchers working with the TRISM LST dataset.

Lastly, we have refined the validation and comparison sections of the manuscript. Our intention with these revisions was to improve the quality of the TRIMS LST dataset and enhance the overall readability of the paper. We sincerely appreciate the time and effort you put into editing and reviewing the manuscript. Your valuable input has played a significant role in improving both the dataset and the manuscript. We are looking forward to collaborating with you to bring the manuscript closer to publication in Earth System Science Data.

Sincerely,

Wenbin Tang and co-authors

University of Electronic Science and Technology of China

wenbint@std.uestc.edu.cn

## Reviewer #1:

Dear Editor,

The manuscript reported a daily 1-km all-weather LST dataset for the Chinese landmass and surrounding areas from 2000 to 2021 with the special features of the longest time coverage, high image quality, and good accuracy. The study is interesting and fits within the scope of "Earth System Science Data".

The main concept of the paper (the necessity to obtain long time-series all-weather LST from 2000 to 2021, especially during the temporal gaps of MODIS between 2000 and 2002) is well presented and introduced. The objective for work is laid out clearly in the introduction section.

The adopted approaches and methodologies are detailed, and sound and the supporting visual material is useful to better understand the exposed concepts. The experimental setup for the data acquisition and data processing is well structured and presented.

The results comprehensively demonstrates the data quality of TRIMS LST by comparison with reanalysis data, satellite TIR LST products, validation against *in-situ* LST, and quantification of the similarity between the TRIMS-Aqua LST and TRIMS-Terra LST time series during the temporal gaps.

Therefore, for final publication, I recommend the manuscript could be accepted after reviewed by editor.

Sincerely

**Authors' response:**

Thank you for your affirmation and praise for our work.

We will continue to improve the method of estimating all-weather land surface temperature and continue to release the latest TRIMS LST publicly.

# Reviewer #2:

## General Comment:

This proposed manuscript produces a daily (four records per day) 1-km all-weather land surface temperature (LST) dataset over China by integrating MODIS Terra, Aqua, and GLDAS reanalysis LSTs from 2000 to 2021. The product after 2002 is produced based on Zhang et al. (2021), and the key contribution of the proposed work is to fill the satellite operation gap from Jan to Feb 2000 for MODIS Terra using random forest (RF) - based extrapolation; the period, Jan 2000 to Jul 2002, for MODIS Aqua LST, is recovered referring to Terra LST in the same period. The core assumption of the proposed algorithm is that the trained RF model from Terra LST with meteorological factors can be directly used for Aqua LST. Overall, such a contribution is expected to be of interest to the community, particularly compared to the published all-weather LST datasets that typically start from 2002. However, there are some concerns regarding the RF modeling approach, theoretical flaws in the core assumption, and lack of site validation for the proposed algorithm. While the assessment of the product generated after 2002 appears to be sound, there are reservations about the proposed method and the validation of this gap period, which do not appear to be convincing.

**Authors' response:**

Thank you for your valuable feedback for recognizing the professional and scientific tone of our paper. We acknowledge that there is room for improvement in the RF modeling details, theoretical flaws in the core assumption, and lack of site validation for the RFSTM/TSETR method. We have taken your concerns seriously and have revised the methodology, results and discussion sections, as well as other parts of our paper based on your comment, to address the issue of method credibility and ensure that the TRISM LST are more credible. Please see our responses below. (The changes are highlighted in red in our revised manuscript.).

## Major

### (1) Comment 1

In Module III (Section 3.3), it is assumed that the random forest model, trained on Terra LST (morning time), can be directly applied to Aqua LST at noon time to calculate both the LFC (Eq. 5) and HFC (Eq. 6). I have concerns about the validity of this assumption. Based on my understanding of Zhang et al. (2021), the HFC is used to adjust the initially reconstructed LSTs for each day from the averaged passing time (~10:30 am) in a year to the actual passing time (see Figure 2 of Zhang et al).

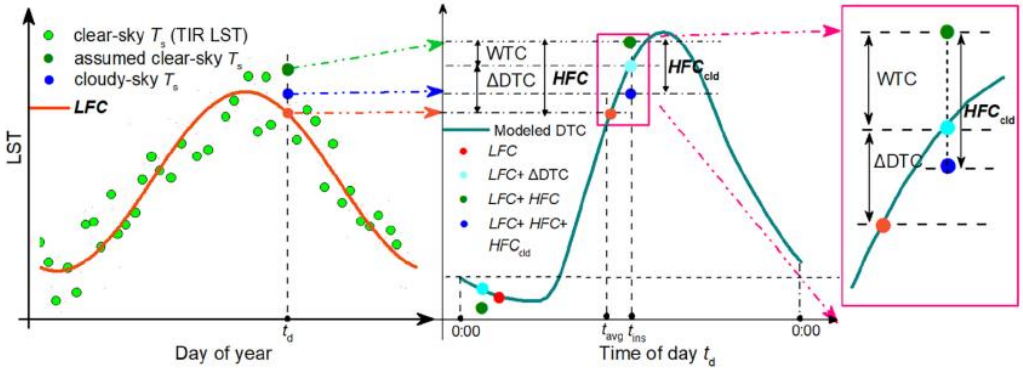


Fig. 2A. Diagram of LST time series decomposition of a 1-km pixel on DOY td of a year. In this diagram, the pixel is under cloudy conditions at tins (i.e., the observation time of a TIR sensor). Please note that the deep blue circle denotes the true cloudy LST at tins on DOY td while the deep green circle denotes the corresponding assumed clear LST. Also note that HFCcld can be positive or negative. (For interpretation of the references to colour in this figure legend, the reader is referred to the web version of this article.)

And such conversion utilized RF modeling, based on location and terrain information, NDVI, water vapor, and time difference for Terra LSTs. And the model was then directly applied for Aqua for the corresponding period, and I think it is not convincing because：

1) around Terra's passing time, the warming rate should be high in a day, while at Aqua's passing time, the temperature reaches its peak at noon, which is relatively stable. Thus, LST in the morning is statistically more sensitive to the time difference, and the

morning model should also be sensitive to ΔT while when it is used for Aqua data, things are different.

2) The model (Eq. 6) used in the morning does not take into account the dominant role of solar radiation in warming, which may affect its accuracy when applied to Aqua LST.

Additionally, 3) LST should have quite different sensitivities to the factors in Eq. 6 at both morning and noon times. Therefore, the direct application of the Terra-trained random forest model to Aqua LST may not be correct in theory. Even though some of the previous studies have assumptions to connect Terra and Aqua LSTs, they may not build models in the way as this paper.

In Eq. 8, cloud cover correction for Aqua LST is performed using an RF model that is trained on LST and meteorological factors at Terra time. However, I have concerns about the applicability of the morning model to noon time.

1) GLDAS temperatures, which are essential inputs for the model, exhibit significantly different bias magnitudes at different times of the day. Therefore, it is questionable whether the model trained in the morning can be used for noon time.

2) In addition, cloud conditions can change substantially throughout the day, including changes in cloud cover and cloud types. The statistical relationship used in the RF model may not adequately reflect such changes, and further validation is required to ensure its accuracy.

3) Moreover, the importance of different factors that affect LST may differ between morning and noon times. In the morning, LST warming is mainly controlled by solar radiation, while at noon time, when solar radiation is sufficient, the peak temperature may be highly affected by water vapor. Therefore, it is necessary to consider these factors when applying the cloud cover correction method.

**Authors' response:**

Thanks very much for your thoughtful comment.

To begin, we explain the calculation process of the LFC (Eq. 5). As shown in Fig. 2A, according to Zhan et al. (2014), a clear daytime (or nighttime) LST time series of

a year can be generally decomposed into three components (Fig.2A). ATC denotes an ideal clear LST variation at the intra-annual average observation time of a TIR sensor due to the Earth revolution corresponding to inclination of the Earth's axis to the ecliptic. Given that latter two components are at a higher frequency compared to ATC, they are hereafter termed as high-frequency components (HFC) and ATC is termed as low-frequency component (LFC). According to the analytical expression and physical meaning of LFC, there is no underlying trends of change within the three annual parameters ($T_{avg}$, $A$ and $\omega$) except for the periodic variation in the LST, which means that the LFC is **cyclic-stationary** over a short time period (Bechtel, 2015; Weng and Fu, 2014; Zhu et al., 2022). Once the three annual parameters are determined, the LFC can be calculated for a given day. Therefore, in TSETR method, we assume that the LFC differences (ΔLFC) between the Terra and Aqua overpass times in T1 and T2 are also cyclic-stationary (Fig.2B). Using Eq. (5), we can calculate the LFC for Aqua LST in the T1 time period.

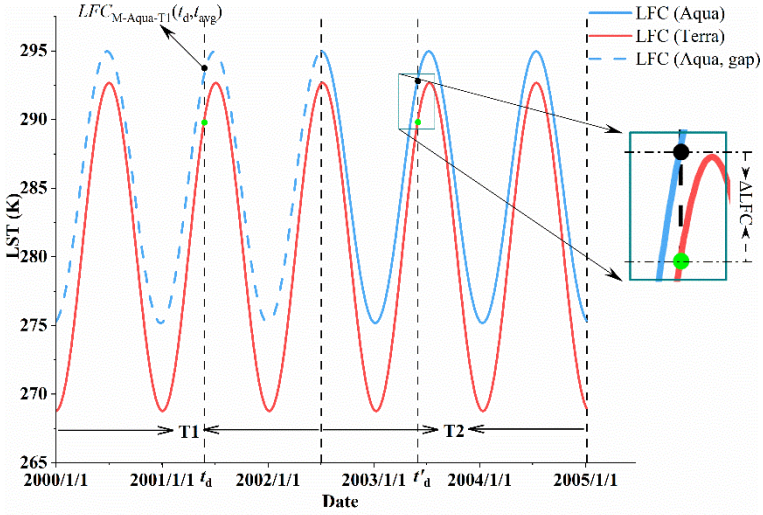


Fig.2B: Schematic diagram for estimating *LFC* in T1.

Then, we totally agree with you that the assumption of applying a Terra-trained random forest model directly to Aqua LST should be further discussed. HFC represents the LST change between $t_{avg}$ and $t_{ins}$ due to the Earth's rotation under clear conditions. So far, there is no available physical model to determine HFC from remote sensing observations due to the impossibility of satisfying the input requirement of the HFC-

involved land surface models. However, there is a potential solution. As pointed out by Zhan et al. (2012; 2014), it is reasonable to describe HFC using its descriptors through empirical or implicit functions.

For the following reasons, $f_{M\text{-}Terra\text{-}T1}$ in Eq. (6) can be utilized to estimate the Aqua transit time HFC. Firstly, the LST of the same pixel at different time points during a given day satisfies the standard conditions of similar pixels in the RTM method (Zhang et al., 2021). This forms the theoretical foundation for the conversion between Terra/MODIS LST and Aqua/MODIS LST (Li et al., 2018). Moreover, considering the meaning of HFC and the parameterization scheme, a strong correlation is expected to exist between similar pixels. Secondly, the factors employed to construct the mapping model effectively capture the impact of diurnal LST variation ($\Delta t_{\mathrm{M}}$) and weather variation ($v_{\mathrm{M}}$).

However, the paucity of HFC estimation studies has led us to overlook a key issue you raise: the difference in timing of Terra and Aqua observations, which leads to a different pattern of LST changes. The observation time of Terra usually varies between 10:00 am and 12:00 pm local solar time. Duan et al. (2014a) showed that the LST varies linearly from 10:00 am to 12:00 pm local solar time. In contrast, Aqua has a nonlinear change of LST over the observation period, as shown by the DTC curves (Duan et al., 2014b; Jin and Dickinson, 1999). Hence, Eq. (6) needs improvement.

In the RTM method, the HFC of similar pixels (S) of a target pixel (M) can be obtained from the MODIS LST:

$$HFC_{\mathrm{s}_n}(t_{\mathrm{d}}, t_{\mathrm{ins}}) = T_{\mathrm{m-S}_n}(t_{\mathrm{d}}, t_{\mathrm{ins}}) - LFC_{\mathrm{m-S}_n}(t_{\mathrm{d}}, t_{\mathrm{avg}}) \quad (2\mathrm{A})$$

where $\mathrm{S}_n$ is the n-th similar pixel of M; $T_{\mathrm{m}}$ and $LFC_{\mathrm{m}}$ are the MODIS LST of S and LFC of the similar pixel, respectively.

On this basis, the HFC of a similar pixel S can be expressed as:

$$HFC_{\mathrm{S}}(t_{\mathrm{d}}, t_{\mathrm{ins}}) = \mathbf{RF}(lat_{\mathrm{S}}, lon_{\mathrm{S}}, DEM_{\mathrm{S}}, NDVI_{\mathrm{S}}, slp_{\mathrm{S}}, \alpha_{\mathrm{S}}, \theta_{\mathrm{s\text{-}S}}, \theta_{\mathrm{m\text{-}S}}, \Delta t_{\mathrm{S}}, v_{\mathrm{S}}) + \varepsilon \quad (2\mathrm{B})$$

where $\mathrm{S}_n \in \mathrm{S} \subseteq \mathrm{W1}$

where $lat$，$lon$，$DEM$，$NDVI$，$slp$，$\alpha$，$\theta_{\mathrm{s}}$，$\theta_{\mathrm{m}}$, $\Delta t$, and $\Delta v$ are latitude, longitude, DEM, NDVI, slope, surface albedo, solar zenith angle, MODIS observation angle, difference

between instantaneous and intraannual average observation time of MODIS, and atmospheric water vapor, respectively. If the descriptors in this equation accurately and adequately describe the situation, the approximation error ε can be minimized.

At this stage, the RF, which is built using the similar image element S, can be readily employed to estimate the HFC of the target pixel M:

$$HFC_{\mathrm{M}}(t_{\mathrm{d}},t_{\mathrm{ins}}) = \mathbf{RF}(lat_{\mathrm{M}},lon_{\mathrm{M}},DEM_{\mathrm{M}},NDVI_{\mathrm{M}}(t_{\mathrm{d}}), slp_{\mathrm{M}}(t_{\mathrm{d}}),\alpha_{\mathrm{M}}(t_{\mathrm{d}}),\theta_{\mathrm{s\text{-}M}}(t_{\mathrm{d}}),\theta_{\mathrm{m\text{-}M}}(t_{\mathrm{d}}),\Delta t_{\mathrm{M}}(t_{\mathrm{d}}),v_{\mathrm{M}}(t_{\mathrm{d}})) \quad (2\mathrm{C})$$

According to Eq. (2A), a prerequisite for obtaining HFC is that a certain number of Aqua/MODIS LSTs are needed as training samples. However, Aqua/MODIS LSTs are not available for the period from DOY 1 of 2000 to DOY 184 of 2002. **With Module I and Module II, we have obtained TRIMS-Terra LSTs for the period T1, which provide the opportunity to establish a transformation relation to obtain the Aqua/HFC.**

The accuracy of the HFC estimates is not affected by the omission of solar radiation's dominant role in warming in Eq. (2C). This is mainly due to the use of Aqua MODIS LST in the modelling, which directly provides information on the peak (daytime) LST. Additionally, during this time interval, temporal gradient of DTC is approximately its minimum.

When there is no valid Aqua LST available, we can enhance Eq. (6) as follows：

$$\begin{cases} HFC_{\text{M-Aq-T1}}(t_{\mathrm{d}},t_{\text{ins-T1}}) = HFC_{\text{M-Te-T1}}(t_{\mathrm{d}},t_{\text{ins-T1}}) + \Delta HFC_{\text{M-Te-Aq-T1}}(t_{\mathrm{d}},t_{\text{ins-T1}}) \\ \Delta HFC_{\text{M-Te-Aq-T1}}(t_{\mathrm{d}},t_{\text{ins-T1}}) = \mathrm{f}_{\text{M-T2}}(g_{\mathrm{M}},DEM_{\mathrm{M}},NDVI_{\mathrm{M}}(t_{\mathrm{d}}),slp_{\mathrm{M}}(t_{\mathrm{d}}),\alpha_{\mathrm{M}}(t_{\mathrm{d}}),v_{\mathrm{M}}(t_{\mathrm{d}}),\Delta LFC_{\mathrm{M}},\Delta DTC_{\mathrm{M}}) \\ \Delta DTC_{\mathrm{M}} = \Delta DTC_{\text{M-Aq}}(t_{\mathrm{d}},t_{\text{ins-T1}},t_{\text{avg-T1}}) - \Delta DTC_{\text{M-Te}}(t_{\mathrm{d}},t_{\text{ins-T1}},t_{\text{avg-T1}}) \end{cases} \quad (2\mathrm{D})$$

where ΔLFC characterizes the systematic deviation of the steady state component, ΔDTC characterizes the warming effect of solar radiation, and the weather effect can be characterized by the atmospheric water vapor content. According to Zhang et al. (2021), the HFC characterizes the change in LFC with ΔDTC and WTC superimposed under ideal clear-sky conditions. The detailed calculation of ΔDTC can be found in Zhang et al. (2019).

The $f_{M\text{-}T2}$ is constructed as follows:

Initially, the correlation image of the target pixel M is determined within the T2 time period, following two conditions need to be satisfied by the correlation image: i) the MBD of the DTC estimated from its corresponding GLDAS LST (10:00-14:00 and 21:00-3:00 local time) should be less than 1.0 K, and ii) the difference in the average observation time between the GLDAS pixels should not exceed 0.5 h. Subsequently, in the correlation image, using similar land surface type criteria, the similar image family S of the target pixel M within the GLDAS pixels is identified. S needs to meet the following two conditions: (i) it should have the same land surface type as M and (ii) the correlation coefficients of the Terra-MODIS LST time series corresponding to S and M need to be greater than 0.8.

Finally, we improved the method described in Eq. (8) of the original manuscript. The aim of this technique is to obtain the initial 1km all-weather LST, which results in $LST_{\text{M-G-Aqua-T1}}$. In this stage, we need to estimate the $HFC_{\text{cld}}$ within the temporal gap period at the Aqua overpass time. In fact, $HFC_{\text{cld}}$ is essentially an atmospheric correction term and it is obtained from the GLDAS LST in the RTM method. According to the parameterization scheme of the RTM method, the clear-sky MODIS pixels and their corresponding GLDAS LSTs are the necessary inputs for the estimation of $HFC_{\text{cld}}$. It is not possible to obtain $HFC_{\text{cld}}$ directly in this stage due to the lack of Aqua/MODIS in T1. We have modified the method of acquiring the initial 1km all-weather LST. Initially, the GLDAS LSTs that corresponded to the Aqua overpass time are corrected for systematic bias using CDF matching. In T1 time period, since Aqua LST data is unavailable, we employee MODIS LST from 2003-2022 to guarantee an adequately large sample of MODIS LST. We then downscaled the GLDAS LST to 1 km resolution by the following two steps:

(i) Calculating the LST differences for the MODIS and GLDAS:

$$\begin{cases} \Delta LST_{\text{M-G-Auqa-T1}}(t_{\text{d}}, t_{\text{ins}}) = LST_{\text{G-Auqa-T1}}(t_{\text{d}}, t_{\text{ins}}) - LST_{\text{M-Auqa-T1}}(t_{\text{d}}, t_{\text{ins}}) \\ LST_{\text{M-Auqa-T1}}(t_{\text{d}}, t_{\text{ins}}) = LFC_{\text{M-Auqa-T1}}(t_{\text{d}}, t_{\text{ins}}) + HFC_{\text{M-Auqa-T1}}(t_{\text{d}}, t_{\text{ins}}) \end{cases} \quad (2\text{E})$$

where $LST_{\text{G-Aqua-T1}}$ is GLDAS LST; $LST_{\text{M-Aqua-T1}}$ is ideal MODIS clear-sky LST. $LST_{\text{M-G-Aqua-T1}}$ is LST difference image. One pixel in GLDAS LST corresponds to 625 (25 × 25) pixels in MODIS LST. The LST differences are calculated as GLDAS LST minus

625-pixel average MODIS LST. LST difference image was then directly resampled to 1 km resolution.

(ii) Developing downscaled GLDAS LST:

$$LST_{\text{M-G-Auqa-T1}}(t_{\text{d}}, t_{\text{ins}}) = \Delta LST_{\text{M-G-Auqa-T1}}(t_{\text{d}}, t_{\text{ins}}) + LST_{\text{M-Auqa-T1}}(t_{\text{d}}, t_{\text{ins}}) \quad (2\text{F})$$

where $LST_{\text{M-G-Aqua-T1}}$ is the initial 1-km downscaled GLDAS LST. Because MODIS LST can reflect the heterogeneity of the underlying land surface within a 0.25°grid, so can the downscaled GLDAS LST (Yao et al.,2023). This is based on the hypothesis that the spatial variations in MODIS LST is the same as that of GLDAS LST.

**After considering your suggestion in Comment 3, we tested the enhanced TSETR method using field validation and intercomparison (Table 2A and 2B). Overall, the results indicate that the accuracy of TSETR is similar to that of the RTM method, thereby increasing the confidence in gap period.**

Reference:

Bechtel, B.: A New Global Climatology of Annual Land Surface Temperature, Remote Sensing, 7, 2850–2870, https://doi.org/10.3390/rs70302850, 2015.

Duan, S.-B., Li, Z.-L., Tang, B.-H., Wu, H., and Tang, R.: Generation of a time-consistent land surface temperature product from MODIS data, Remote Sens. Environ., 140, 339–349, https://doi.org/10.1016/j.rse.2013.09.003, 2014a.

Duan, S.-B., Li, Z.-L., Tang, B.-H., Wu, H., Tang, R., Bi, Y., and Zhou, G.: Estimation of Diurnal Cycle of Land Surface Temperature at High Temporal and Spatial Resolution from Clear-Sky MODIS Data, Remote Sens., 6, 3247–3262, https://doi.org/10.3390/rs6043247, 2014b.

Jin, M. and Dickinson, R. E.: Interpolation of surface radiative temperature measured from polar orbiting satellites to a diurnal cycle: 1. Without clouds, Journal of Geophysical Research: Atmospheres, 104, 2105–2116, https://doi.org/10.1029/1998JD200005, 1999.

Li, X., Zhou, Y., Asrar, G. R., and Zhu, Z.: Creating a seamless 1km resolution daily land surface temperature dataset for urban and surrounding areas in the conterminous United States, Remote Sensing of Environment, 206, 84–97,

https://doi.org/10.1016/j.rse.2017.12.010, 2018.

Long, D., Yan, L., Bai, L., Zhang, C., Li, X., Lei, H., Yang, H., Tian, F., Zeng, C., Meng, X., and Shi, C.: Generation of MODIS-like land surface temperatures under all-weather conditions based on a data fusion approach, Remote Sensing of Environment, 246, 111863, https://doi.org/10.1016/j.rse.2020.111863, 2020.

Weng, Q. and Fu, P.: Modeling annual parameters of clear-sky land surface temperature variations and evaluating the impact of cloud cover using time series of Landsat TIR data, Remote Sensing of Environment, 140, 267–278, https://doi.org/10.1016/j.rse.2013.09.002, 2014.

Yao, R., Wang, L., Huang, X., Cao, Q., Wei, J., He, P., Wang, S., and Wang, L.: Global seamless and high-resolution temperature dataset (GSHTD), 2001–2020, Remote Sensing of Environment, 286, 113422, https://doi.org/10.1016/j.rse.2022.113422, 2023.

Zhan, W., Chen, Y., Voogt, J. A., Zhou, J., Wang, J., Ma, W., and Liu, W.: Assessment of thermal anisotropy on remote estimation of urban thermal inertia, Remote Sensing of Environment, 123, 12–24, https://doi.org/10.1016/j.rse.2012.03.001, 2012.

Zhan, W., Zhou, J., Ju, W., Li, M., Sandholt, I., Voogt, J., and Yu, C.: Remotely sensed soil temperatures beneath snow-free skin-surface using thermal observations from tandem polar-orbiting satellites: An analytical three-time-scale model, Remote Sensing of Environment, 143, 1–14, https://doi.org/10.1016/j.rse.2013.12.004, 2014.

Zhang, X., Zhou, J., Göttsche, F.-M., Zhan, W., Liu, S., and Cao, R.: A Method Based on Temporal Component Decomposition for Estimating 1-km All-Weather Land Surface Temperature by Merging Satellite Thermal Infrared and Passive Microwave Observations, IEEE Transactions on Geoscience and Remote Sensing, 57, 4670–4691, https://doi.org/10.1109/TGRS.2019.2892417, 2019.

Zhang, X., Zhou, J., Liang, S., and Wang, D.: A practical reanalysis data and thermal infrared remote sensing data merging (RTM) method for reconstruction of a 1-km all-weather land surface temperature, Remote Sensing of Environment, 260,

112437, https://doi.org/10.1016/j.rse.2021.112437, 2021.

Zhu, X., Duan, S.-B., Li, Z.-L., Wu, P., Wu, H., Zhao, W., and Qian, Y.: Reconstruction of land surface temperature under cloudy conditions from Landsat 8 data using annual temperature cycle model, Remote Sensing of Environment, 281, 113261, https://doi.org/10.1016/j.rse.2022.113261, 2022.

**(2) Comment 2**

**RF modeling details**

The proposed method utilized RF modeling several times but in many different ways: Module II extrapolate the Terra LST to Jan 01 2000 by learning the relationship between LST and factors (e.g., DEM, NDVI, soil moisture). Module III reconstructs Aqua LST based on the relationship of Terra LST with environmental factors.

The first question is how the RF model is trained. Did you build one generic model that is applied to all pixels over China? Or several subset models for different climate zones or land cover types? I do not see any description of the RF model training introduction, how the training data is sampled, or how the model is tested, even though RF modeling has been used in every step.

In addition, one-year (2000.03 – 2001.02) data for training is not enough (in theory) as the drought condition may change considerably year by year due to the climate's internal variability.

Did you separate samples for daytime and nighttime? Factors (e.g., albedo) should play different roles in daytime and nighttime.

Driving factors from GLDAS is three-hourly, and how did such coarse time resolution impact your modeling accuracy? Which interpolation methods did you use?

**Authors' response:**

Thanks for your comments.

(i) RF parameters: To determine the optimal parameters, we follow a two-step process. First, we define a large range for each hyperparameter to be optimized. For example, we may define a range of 10 to 5000 for the hyperparameter "n estimators." Next, we use an optimization algorithm to search for the optimal value of each

hyperparameter within this range. This involves performing multiple cross-validations for each parameter combination within the specified range and selecting the combination with the highest average score as the optimal parameter. However, this method becomes inefficient when dealing with large datasets. To address this issue, we employ a two-step approach combining random search and grid search. Initially, we use random search to obtain a set of parameters that can serve as a reference for subsequent grid search. Eventually, by using the grid search method, we determine the optimal parameters. **In module II, the model parameters were set as follows: n estimators = 420, max depth = 43, max features = 9, and min samples leaf = 1. In module I and module III，the model parameters were set as follows: n estimators = 100, max depth = 20, max feature = 4, min samples leaf = 1.**

(ii) RF model building: In the temporal stage of RFSTM, all-weather samples from **2000 to 2005** were compiled. Usually, in RF algorithm, approximately two-thirds of the samples are used for model training and the remaining are for model validation (Breiman, 2001). The temporal descriptors of LST include net longwave radiation, downward longwave flux, soil moisture profile (e.g., surface, 0-10 cm and 10-40 cm in GLDAS NOAH model-based data), wind-speed, soil temperature profile (e.g., surface, 0-10cm and 10-40 cm in GLDAS NOAH-model based data), air temperature and albedo. In spatial stage, RF is trained with the 1-km LST and spatial descriptors of a similar day, and which (i) has the same observation time as $t_d$; (ii) has the smallest difference in the number of days between $t_d$. For a specific day ($t_d$), classify he study area into several subareas, including thick vegetation (NDVI>0.5), sparse vegetation ($0.2 \leq$ NDVI $\leq 0.5$), barren land areas (NDVI < 0.2), snow-ice areas (NDSI>0.1) (Zhang et al., 2019) and water (NDVI<0), using the1-km NDVI (Sobrino et al.,2004) and NDSI. **For each subarea, upscale the resolution of spatial descriptors to 0.25° to match the GLDAS LST. Then train the RF regression relationship (i.e., $f_S$) between the GLDAS LST and the spatial descriptors over the clear-sky and the cloudy area, respectively**, via Eq. (3). Note that only GLDAS grids with more than 80% subpixels are selected for training during the step. **All RF models are built separately for each of the four MODIS overpass time.**

(iii) Other: The selected temporal descriptors from GLDAS data are temporally interpolated using **cubic spline function** to observation time of MODIS LST for the purpose of temporal-matching. The results of Zhang et al. (2021) and Table 2A have shown that the effect of interpolation on the accuracy of the merged LSTs **is limited**, although the LDAS data is 3 hour for GLDAS.

Reference:

Breiman, L.: Random Forests, Machine Learning, 45, 5–32, https://doi.org/10.1023/A:1010933404324, 2001.

Sobrino, J. A., Jimenez-Munoz, J. C., and Paolini, L.: Land surface temperature retrieval from LANDSAT TM 5, Remote Sens. Environ., 90, 434–440, https://doi.org/10.1016/j.rse.2004.02.003, 2004.

Zhang, H., Zhang, F., Zhang, G., Che, T., Yan, W., Ye, M., and Ma, N.: Ground-based evaluation of MODIS snow cover product V6 across China: Implications for the selection of NDSI threshold, Science of The Total Environment, 651, 2712–2726, https://doi.org/10.1016/j.scitotenv.2018.10.128, 2019.

Zhang, X., Zhou, J., Liang, S., and Wang, D.: A practical reanalysis data and thermal infrared remote sensing data merging (RTM) method for reconstruction of a 1-km all-weather land surface temperature, Remote Sensing of Environment, 260, 112437, https://doi.org/10.1016/j.rse.2021.112437, 2021.

**(3) Comment 3**

**Independent site validation does not cover 2000-2002**

This is also a serious issue, and only the spatial comparison with ERA5 and GLDAS is not enough for claiming the proposed algorithm is ready for production. Independent ground validation is still necessary. Suggest either collecting more site data for assessment or assuming 2003-04 are missing and recovering these two years by the same model you trained in module II and module III. And then the site validation and inter-comparison with Zhang et al (2021) can be done.

You may also try cross-validation of module II and III to check which module is most

robust. Essentially, both modules II and III can recover Aqua LST before 2002.07.

**Authors' response:**

Thanks very much for your thoughtful comment.

Regrettably, during T1 period, there are no independent ground stations available. Observations of D105 and GAZ commenced on the **DOY275 of 2002 (2 October).**

To investigate the generalization ability of the RFSTM at the temporal dimension, the method is implemented from following: **For 2003, the GLDAS and Terra MODIS data are also merged to generate 1-km TRIMS-Terra LST.**

This study utilized the method to reconstruct the TRIMS-Aqua LST over a period of 915 days. To ensure a comprehensive analysis, **TRIMS-Aqua LSTs for 2003(DOY1)-2005(DOY185) and 2013(DOY1)-2015(DOY185)** were generated using method. This allowed for the inclusion of a significant number of independent ground stations for validation purposes.

Table 2A shows the results of the comparison between the TRIMS-Terra LST generated by the RFSTM-based method the RTM-based method.

Table 2A: MBE, and RMSE from validation results of TRIMS-Terra LST with the in-situ LST

| Site | Condition | TRIMS-Terra LST (RTM) | | | | TRIMS-Terra LST (RFSTM) | | | |
|---|---|---|---|---|---|---|---|---|---|
| | | Daytime | | Nighttime | | Daytime | | Nighttime | |
| | | MBE (K) | RMSE (K) | MBE (K) | RMSE (K) | MBE (K) | RMSE (K) | MBE (K) | RMSE (K) |
| D105 | All | 1.63 | 3.15 | -1.05 | 1.94 | 1.75 | 3.3 | -1.55 | 2.20 |
| | clear | 1.78 | 2.17 | -1.17 | 2.04 | 1.85 | 3.34 | -2.37 | 2.66 |
| | cloudy | 1.54 | 3.25 | -0.88 | 1.78 | 1.04 | 3.44 | -0.40 | 1.29 |
| GZA | All | 0.93 | 2.61 | -0.78 | 1.76 | 1.26 | 3.10 | -1.95 | 2.26 |
| | clear | 0.79 | 2.51 | -0.68 | 1.70 | 0.94 | 2.72 | -1.26 | 2.10 |
| | cloudy | 1.11 | 3.71 | -0.94 | 1.85 | 1.61 | 4.20 | -1.47 | 2.35 |

Table 2A shows that TRIMS-Terra LST generated by the RTM method and RFSTM method have similar accuracies. MBEs have a difference of less than 0.50 K, and RMSEs have a difference of less than 1.2 K. Overall, the RFSTM method is slightly less accurate than the TRIMS-Terra LST generated by the RTM method. **It is to be observed that the RFSTM method was only used to generate LST for a period of**

**53 days, which has a relatively smaller impact on the overall accuracy of TRIMS LST.**

Table 2B shows the results of the comparison between the TRIMS-Aqua LST generated by the TSETR-based method and the RTM-based method.

Table 2B: MBE, and RMSE from validation results of TRIMS-Aqua LST with the in-situ LST

| Site | Condition | TRIMS-Aqua LST (RTM) | | | | TRIMS-Aqua LST (TSETR) | | | |
|---|---|---|---|---|---|---|---|---|---|
| | | Daytime | | Nighttime | | Daytime | | Nighttime | |
| | | MBE (K) | RMSE (K) | MBE (K) | RMSE (K) | MBE (K) | RMSE (K) | MBE (K) | RMSE (K) |
| ARO | All | -0.53 | 2.14 | 0.58 | 1.77 | -0.75 | 2.38 | 0.64 | 2.17 |
| | clear | -0.47 | 2.11 | 0.52 | 1.74 | -0.63 | 2.35 | 0.75 | 2.25 |
| | cloudy | -0.57 | 2.16 | 0.70 | 1.81 | -0.87 | 2.34 | 0.88 | 1.85 |
| DAM | All | -0.24 | 2.06 | 0.55 | 1.81 | -0.38 | 2.47 | 0.60 | 1.84 |
| | clear | -0.28 | 2.03 | 0.52 | 1.81 | -0.45 | 2.61 | 0.53 | 2.03 |
| | cloudy | -0.23 | 2.09 | 0.56 | 1.82 | -0.30 | 2.73 | 0.76 | 2.32 |
| D105 | All | 0.80 | 2.67 | -1.01 | 1.77 | 1.11 | 2.31 | -1.15 | 1.88 |
| | clear | 1.55 | 3.05 | -0.94 | 1.71 | 1.87 | 3.22 | -1.37 | 1.86 |
| | cloudy | 0.59 | 2.54 | -1.09 | 1.85 | 0.45 | 1.96 | -0.63 | 1.22 |
| GZA | All | -0.74 | 2.73 | -0.67 | 1.51 | -0.93 | 3.01 | -1.08 | 2.09 |
| | clear | -0.60 | 2.61 | -0.65 | 1.48 | -0.98 | 2.74 | -0.68 | 1.83 |
| | cloudy | -0.93 | 2.89 | -0.73 | 1.60 | -1.05 | 3.29 | -0.94 | 2.24 |
| GOB | All | -0.34 | 2.60 | 0.21 | 1.87 | -0.62 | 2.77 | 0.47 | 2.15 |
| | clear | 1.88 | 2.41 | 1.64 | 1.93 | 1.77 | 2.76 | 1.66 | 2.04 |
| | cloudy | -2.31 | 2.75 | -1.51 | 1.79 | -2.63 | 2.84 | -1.79 | 2.45 |
| SDQ | All | -0.27 | 2.41 | 0.93 | 1.78 | -0.59 | 2.75 | 1.23 | 2.40 |
| | clear | -0.18 | 2.37 | 0.97 | 1.80 | -0.19 | 2.09 | 1.26 | 2.19 |
| | cloudy | -0.39 | 2.46 | 0.87 | 1.74 | -0.81 | 2.88 | 1.17 | 2.37 |

The TRIMS-Aqua LST generated by the TSETR method and the RTM method have similar accuracies, with the MBE differing by no more than 0.40 K and the RMSE differing by no more than 0.7 K. Combining the results of Table 2A and 2sB, the TSETR method still shows high accuracy and stability when generating LST over longer time periods. Therefore, it can be assumed that the TRIMS-Aqua LST in the T1 period reconstructed using the TSETR method also has reasonable accuracy.

## Other Concerns

### (4) Comment 4

Table 1: site representativeness of fluxes should be highly related to the observing height and local terrain; however, comparing SDQ to D105 and GAZ, even D105 and GAZ have very low heights and high elevation, they have similar $u_{REP}$ with SDQ, can you explain that? What does the '*' mean?

**Authors' response:**

Thanks for your thoughtful comment.

$u_{REP}$ represents the error due to differences in the representativeness of the site's observation field of view and the scale of the satellite pixels. Despite the lower elevation of D105 and GAZ, we found that the land cover types within the FOV of these two sites were consistent with the corresponding 1 km MODIS site pixels. In addition, based on the 30- m Landsat-7 ETM+ LST product for 2002-2004, we found that the mean intra-annual standard deviation of LST within the 1-km MODIS site pixels did not exceed 1.50 K, which is similar to that of the SDQ, and therefore it is reasonable that they have similar $u_{REP}$. While $u_{REP}$ offers a fresh perspective on quantifying site spatial representation, it does not facilitate reader comprehension. Therefore, we opted to convey the spatial representation using STDs instead.

The symbol ('*') indicates that this height is the average height of the instrument above the canopy (Ma et al.,2021). (Please see P7, L165)

Reference:

Ma, J., Zhou, J., Liu, S., Göttsche, F.-M., Zhang, X., Wang, S., and Li, M.: Continuous evaluation of the spatial representativeness of land surface temperature validation sites, Remote Sensing of Environment, 265, 112669, https://doi.org/10.1016/j.rse.2021.112669, 2021.

**(5) Comment 5**

How did you get the albedo and NDVI before the Terra recording time for Module II?

**Authors' response:**

Thank you for your attention to the details of data generation, as it is very important.

We apologize for the lack of explanation and clarification in our manuscript. During the temporal gap (DOY 1–54 2000), SPOT VGT (Toté et al., 2017) served as the NDVI, GLASS albedo was extended to a 1 km resolution using cubic convolution interpolation, and the NDSI was determined by taking the average of the corresponding days in 2001 and 2002.

Reference:

Toté, C., Swinnen, E., Sterckx, S., Clarijs, D., Quang, C., and Maes, R.: Evaluation of the SPOT/VEGETATION Collection 3 reprocessed dataset: Surface reflectances and NDVI, Remote Sensing of Environment, 201, 219–233, https://doi.org/10.1016/j.rse.2017.09.010, 2017.

**(6) Comment 6**

I double-checked the data while it is not standardized, suggest outputting it as NC or HDF file, scaling the matrix, and providing scale factor, and offset, just like MODIS product, which would be easier to be used for modeling input. Write the view time and LST into one file, data quality mark, and cloud mask are also necessary for users. Suggest not compressing the data, even if it is required by the platform, it is better to use ZIP rather than RAR, ZIP is more accessible worldwide.

**Authors' response:**

Thanks very much for your thoughtful comment.

Based on user feedback showing that the GEOTIFF format is easier to use than other common formats, several organizations worldwide have utilized the data since its release in 2019. Due to this feedback and your comment, to enhance user convenience in downloading and using the data, we have converted the compression format to zip and uploaded the TRIMS LST in NETCDF format.

## Minor

**(7) Comment 6**

Line 11: many spatial missing -> many invalid pixels

**Authors' response:**

Thanks for your comment. It has been corrected in the revised manuscript. (P1, L11)

**(8) Comment 8**

Line 16: suggest pointing out four times records per day, which is the strength of this work.

**Authors' response:**

Thanks for your comment. It has been corrected in the revised manuscript. (P1, L16)

**(9) Comment 9**

Line 22: the "temporal gap" should be clarified otherwise it may mislead readers as the gaps caused by cloud cover rather than satellite operation time.

**Authors' response:**

Thanks for your comment. The "temporal gap" is a temporal discontinuity in Terra/Aqua MODIS during the 2000-2002 time period. We have clarified this in the revised manuscript. (P3, L67-69)

**(10) Comment 10**

The quotative analysis part in the abstract should divide the validation for the years after 2002(previous work) and before 2002 (proposed work) because the results after 2002 should be good as it has been peer-reviewed. Further, the bias at Line 27 is huge honestly, suggest also giving the overall statistics rather than the range.

**Authors' response:**

Thanks for your comment. We have tested and validated the methodology used to generate TRIMS LST in T1 as you mentioned in Comment 1 and 3. (P16, Section 3.5; P24-26, Section 4.4)

**(11) Comment 11**

Line 43: “Grain for Green Program” is the official term

**Authors’ response:**

Sorry for this mistake. It has been corrected in the revised manuscript. (P2, L45)

**(12) Comment 12**

Line 71: “regions. LST (Martins et al., 2019).” wrong sentence

**Authors’ response:**

Sorry for this mistake. It has been corrected in the revised manuscript. (P3, L74)

**(13) Comment 13**

Line 72: as ‘a’ physical method

**Authors’ response:**

Sorry for this mistake. It has been corrected in the revised manuscript. (P3, L79)

**(14) Comment 14**

Line 75: MLST-AS should be spelled out, and double-check the whole context for abbr.

**Authors’ response:**

Sorry for this mistake. It has been corrected in the revised manuscript. (P3, L82-83)

**(15) Comment 15**

Line 80: ‘observe LST’ -> ‘retrieve LST’

**Authors’ response:**

Sorry for this mistake. It has been corrected in the revised manuscript. (P3, L92)

**(16) Comment 16**

Line 97: suggest directly specifying the period rather than mentioning ‘outside the temporal gaps’

**Authors’ response:**

Thanks for your comment. We have changed this sentence in the revised. (P4, L105-106)

**(17) Comment 17**

Line 109: space missed in ‘product(’

**Authors’ response:**

Sorry for this mistake. It has been corrected in the revised manuscript. (P4, L117)

**(18) Comment 18**

Line 116-120: as GLDAS is the key input of LST reconstruction here, its LST data should be introduced in detail.

**Authors’ response:**

Thanks for your comment. We have detailed GLDAS LST in a revised version.

The main reanalysis data used in this study are the Global Land Data Assimilation System assimilation (GLDAS) data provided by the Goddard Earth Sciences Data and Information Services Center (GES DISC) (Rodell et al., 2004). GLDAS utilizes an analysis increment, which is obtained through the optimal interpolator using the observed-minus-forecast value for the skin temperature calculated by GLDAS. This analysis increment, along with the bias correction term, is subsequently provided to the land surface models code for energy budget considerations. The bias correction ensures that the modelled state is continually adjusted towards the observed values, thereby improving the accuracy of the skin temperature calculations on an incremental, semi-daily, or daily basis (Radakovich et al., 2001). The accuracy of GLDAS LST has been demonstrated by various studies with MBE ranging from -4.27 K to 8.65 K and RMSE ranging from 3.0 K to 6.02 K (Zhang et al.,2021; Xiao et al.,2023). (P4-5, L129-136)

Reference:

Radakovich, J., Houser, P., Da Silva, A., and Bosilovich, M.: Results From Global Land-surface Data Assimilation Methods, AGU Spring Meeting Abstracts, 1, 2001.

Xiao, Y., Zhao, W., Ma, M., Yu, W., Fan, L., Huang, Y., Sun, X., and Lang, Q.: An Integrated Method for the Generation of Spatio-Temporally Continuous LST Product With MODIS/Terra Observations, IEEE Transactions on Geoscience and Remote Sensing, 61, 1–14, https://doi.org/10.1109/TGRS.2023.3254598, 2023.

Zhang, X., Zhou, J., Liang, S., and Wang, D.: A practical reanalysis data and thermal

infrared remote sensing data merging (RTM) method for reconstruction of a 1-km all-weather land surface temperature, Remote Sensing of Environment, 260, 112437, https://doi.org/10.1016/j.rse.2021.112437, 2021.

**(19) Comment 19**

Table 1: adding a spatial map of sites and land cover types would be great

**Authors' response:**

Thanks for your comment.

We have added illustrations to show the extent of the study area, site locations, and land use types (Figure 2B). (P6)

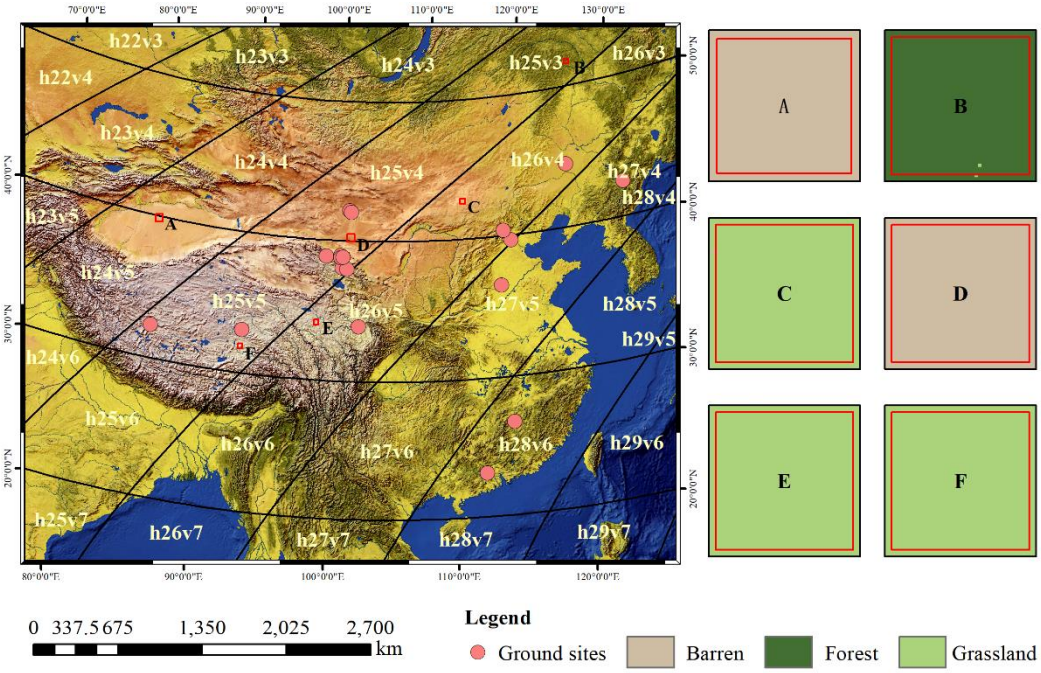


Figure 2B: The study area and the selected 19 ground sites. A, B, C, D, E, and F are subareas exhibited a single land cover type with no change in T1 and T2 (January 1 2000 to January 3 2005)

**(20) Comment 20**

Line 127: literature reference is necessary here for "3% - 10%"

**Authors' response:**

Thanks for your comment. We are very sorry for the oversight. From the information provided in Wang et al (2020), the official web pages of the suppliers and the manuals of the instruments (Fig.2C-2E), we can draw this conclusion: the uncertainty in the

daily totals of the longwave radiation measurements is 3% - 10%.

### 2.1.1 List of specifications of the CNR 1

Specifications of Solar radiation measurement see CM 3 specifications
Specifications of Far Infrared radiation measurement see CG 3 specifications

| | | |
|---|---|---|
| Sensor sensitivities | : | All four sensors have equal sensitivity |
| Pt-100 sensor temperature measurement | : | DIN class A |
| Expected accuracy of the temperature measurement | : | +/- 2 K, under non-stable conditions with solar heating or heating by using the heating resistor. |
| Heating | : | resistor 24 Ohms, 6VA at 12 Volt |
| Expected worst case errors introduced by heating | : | Pyranometer offset 10 Watt per metre square, Pt-100 error of +/- 2K. |
| Stabilisation time for heating | : | 60 minutes |
| Operating temperature | : | -40 to +80 degrees Celsius |
| Requirements for data acquisition | | |
| For Net Radiation only | : | one mV channel |
| For all four components | : | four mV signals, one Pt-100 channel plus software |
| Expected accuracy for daily totals | : | +/- 10 % |
| Cable length | : | 10 m (each cable) |
| Weight | : | 4 kg |
| Options | : | extended cables up to 100 metres<br>2 connectors, connecting the standard 10-meter cables (Radiometer and Pt-100/heater) to the extended cable |

Fig.2C: Instrument information for CNR1 (from the link: https://www.kippzonen.com/Download/85/Manual-CNR-1-Net-Radiometer-English)

KIPP & ZONEN
SINCE 1830

| | | |
|---|---|---|
| Irradiance: | W/m² | 0 to 2000 |
| Definition | | *Measurement range* |
| Non-stability | % | < 1 |
| Definition | | *Maximum change of sensitivity per year, percentage of full scale* |
| Spectral selectivity | % | < 3% (350 – 1500 nm spectral interval) |
| Definition | | *Deviation of the product of spectral absorption and spectral transmittance from the corresponding mean within the indicated spectral range* |
| Uncertainty in daily total | % | < 5 (95 % confidence level) |
| Definition | | *Achievable uncertainty* |
| **International standards** | | |
| ISO | | ISO9060:2018 |
| Instrument calibration | | Indoors, side by side against reference CMP 3 pyranometer according to ISO 9847:1992 annex A.3.1 |

Fig.2D: Instrument information for CNR1 (from the link: https://www.kippzonen.com/Product/85/CNR4-Net-Radiometer)

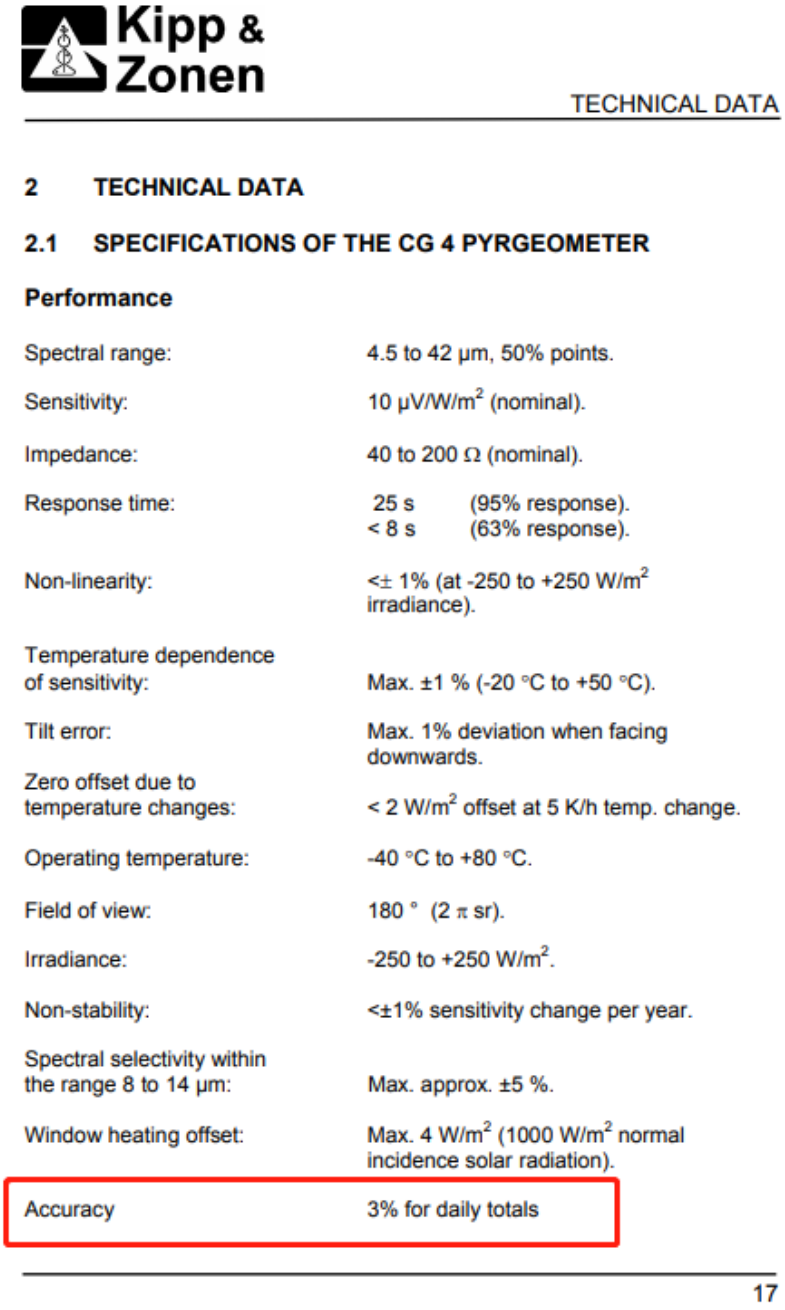

Kipp & Zonen

TECHNICAL DATA

## 2 TECHNICAL DATA

### 2.1 SPECIFICATIONS OF THE CG 4 PYRGEOMETER

**Performance**

| | |
|---|---|
| Spectral range: | 4.5 to 42 µm, 50% points. |
| Sensitivity: | 10 µV/W/m$^2$ (nominal). |
| Impedance: | 40 to 200 Ω (nominal). |
| Response time: | 25 s (95% response).<br>< 8 s (63% response). |
| Non-linearity: | <± 1% (at -250 to +250 W/m$^2$ irradiance). |
| Temperature dependence of sensitivity: | Max. ±1 % (-20 °C to +50 °C). |
| Tilt error: | Max. 1% deviation when facing downwards. |
| Zero offset due to temperature changes: | < 2 W/m$^2$ offset at 5 K/h temp. change. |
| Operating temperature: | -40 °C to +80 °C. |
| Field of view: | 180 ° (2 π sr). |
| Irradiance: | -250 to +250 W/m$^2$. |
| Non-stability: | <±1% sensitivity change per year. |
| Spectral selectivity within the range 8 to 14 µm: | Max. approx. ±5 %. |
| Window heating offset: | Max. 4 W/m$^2$ (1000 W/m$^2$ normal incidence solar radiation). |
| Accuracy | 3% for daily totals |

17

Fig.2E: Instrument information for CNR1 (from the link: https://www.kippzonen.com/Download/33/CG-4-Manual?ShowInfo=true)

Reference:


CNR1 - Net Radiometer: https://www.campbellsci.com/cnr1, last access: 26 June 2023.

CNR4-L - 4-Component Net Radiometer: https://www.campbellsci.com/cnr4, last access: 26 June 2023.

Manual of CG 4 pyrgeometer - Kipp & Zonen: https://www.kippzonen.com/Download/33/CG-4-Manual?ShowInfo=true, last access: 4 August 2023.

Wang, S., Zhou, J., Lei, T., Wu, H., Zhang, X., Ma, J., and Zhong, H.: Estimating Land

Surface Temperature from Satellite Passive Microwave Observations with the Traditional Neural Network, Deep Belief Network, and Convolutional Neural Network, Remote Sensing, 12, 2691, https://doi.org/10.3390/rs12172691, 2020.

**(21) Comment 21**

Line 129: which BBE data do you use for calculating site LST measurements

**Authors' response:**

Thanks for your comment.

According to Stefan–Boltzmann's law, *in-situ* LST can be calculated from the outgoing and incoming longwave radiation, and the BBE was calculated from the emissivities of MODIS（MXD11A1 V61）channels 29, 31, and 32 (Liang,2003)

Reference:

Liang, S. L.: Estimation of Surface Radiation Budget: II. Longwave, in: Quantitative Remote Sensing of Land Surfaces, John Wiley & Sons, Inc, New Jersey, 345–397, https://doi.org/10.1002/047172372X.ch10, 2003.

**(22) Comment 22**

Line 133: Brief introduction of $u_{Rep}$ should be given.

**Authors' response:**

Thanks for your comment. We are sorry for the confusion and unclear description of $u_{Rep}$. In the revised manuscript, we used STD of LST as an indicator of spatial representativeness of site. (P5, L151–155; P7)

**(23) Comment 23**

Line 175, Line 190: suggest replacing 'T-i' to 'T,i' as '–' means minus that will mislead readers, d-1 looks like the day before d.

**Authors' response:**

Thanks for your comment.

It has been corrected in the revised manuscript. (P10, L202, L217)

**(24) Comment 24**

Line 184-185: what is the data source of the factors, how interpolated, why solar radiation is not included, why deep layer soil moisture is included, and is the model

really sensitive to it?

**Authors' response:**

Thanks for your comment.

The selected factors of LST in Module II are listed in Table 2C. The choice of appropriate LST descriptors in the temporal and spatial stage should refer to reasonable correlations of LST to related biophysical variables. In this study, for the temporal stage, LST descriptors are selected based on the theory of the land surface radiation budget in which the longwave net radiation is expressed by following equation (Liang et al., 2010):

$$R_{\mathrm{n}}^{\mathrm{l}} = \varepsilon F_{\mathrm{d}}^{\mathrm{l}} - \sigma \varepsilon T_{\mathrm{s}}^{4} \quad (2\mathrm{G})$$

where $R_{\mathrm{n}}^{\mathrm{l}}$ is net longwave downwelling radiation; $F_{\mathrm{d}}^{\mathrm{l}}$ is long-wave downward fluxes; $\sigma$ is land surface the broad-band emissivity; $\varepsilon$ is Stefan-Boltzmann's constant. Hereby the LST can be derived as:

$$T_{\mathrm{s}} = \left(\frac{R_{\mathrm{n}}^{\mathrm{l}} - \varepsilon F_{\mathrm{d}}^{\mathrm{l}}}{\sigma \varepsilon}\right)^{\frac{1}{4}} \quad (2\mathrm{H})$$

The equation indicates the LST is can be functionally expressed by the net longwave radiation, the long-wave downward fluxes, and the land surface broad-band emissivity. Among these descriptors the former two is obtainable from the reanalysis data while the all-weather emissivity is still unavailable. Therefore, three variables from reanalysis data are selected as emissivity-related descriptors. In addition, three additional LST-related variables (i.e., wind-speed, soil temperature profile, air temperature and albedo) from reanalysis data are selected as ancillary descriptors to consolidate the RF-based mapping in this stage.

For spatial stage, current available 1-km spatial descriptors including surface albedo, latitude and DEM are selected according to Hutengs and Vohland (2016). Note that i) all the descriptors selected in the spatial algorithm is from the ancillary data with the fine resolution (i.e., 1 km in this study); ii) the albedo is selected in this algorithm because it involves the related information of land surface such as vegetation coverage, surface and subsurface moisture and land cover types.

Table 2C. Selected LST descriptors in temporal and spatial algorithms

| **Module II** | **Descriptors** | | |
|---|---|---|---|
| | **Basic descriptor** | **Ancillary descriptor** | **Spatial resolution** |
| **Temporal stage** | net longwave radiation; longwave downward flux; soil moisture profile (e.g., surface, 0–10 cm and 10–40 cm in GLDAS NOAH model-based data); canopy surface water; snow depth water equivalent | wind-speed, soil temperature profile (e.g. surface, 0–10cm and 10–40cm in GLDAS NOAH-model based data); air temperature; albedo | native (coarse) resolution of the reanalysis data used |
| **Spatial stage** | DEM; latitude; albedo | | target (fine) resolution (i.e. 1 km in this study) |

Reference:

Hutengs, C. and Vohland, M.: Downscaling land surface temperatures at regional scales with random forest regression, Remote Sensing of Environment, 178, 127–141, https://doi.org/10.1016/j.rse.2016.03.006, 2016.

**(25) Comment 25**

Line 197: what is the threshold for classification and any reference

**Authors' response:**

Thanks for your comment.

The threshold for classification is referenced from Sobrino et al. (2004) and have been described in the revised manuscript. (P16, L341–343)

**(26) Comment 26**

Line 199-200: hard to read

**Authors' response:**

Sorry for this mistake. It has been corrected in the revised manuscript. (P16, L344–345)

**(27) Comment 27**

Line 217: why DOY 3?

**Authors' response:**

Thanks for your comment.

As shown in the Fig.2F, T2 (DOY 185, 2002 to DOY 3, 2005) is depicted with the same duration as T1.

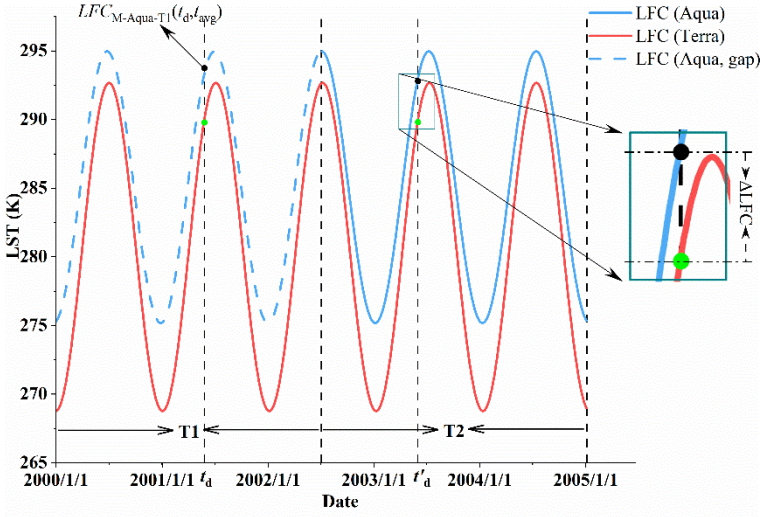


Fig.2F: Schematic diagram for estimating LFC at daytime Aqua overpass time in T1.

**(28) Comment 28**

Line 233: TI -> T1

**Authors' response:**

Thanks for your comment.

It has been corrected in the revised manuscript.

**(29) Comment 29**

Eq. 7: what G means?

**Authors' response:**

Thanks for your comment.

G is the GLDAS pixel containing the target MODIS pixel M

**(30) Comment 30**

Line 310: During the 'temporal gap', there are no Terra or Aqua passing, such statement is misleading and should clarify how the time in this period is determined.

**Authors' response:**

Thanks for your comment.

As the MODIS observation time varies regularly, the observation time during the temporal gap can be obtained by extrapolating from its 16-day cycle. Fig.2G displays the results obtained by recovering the overpass time of cloudy pixels both outside and within the temporal gaps.

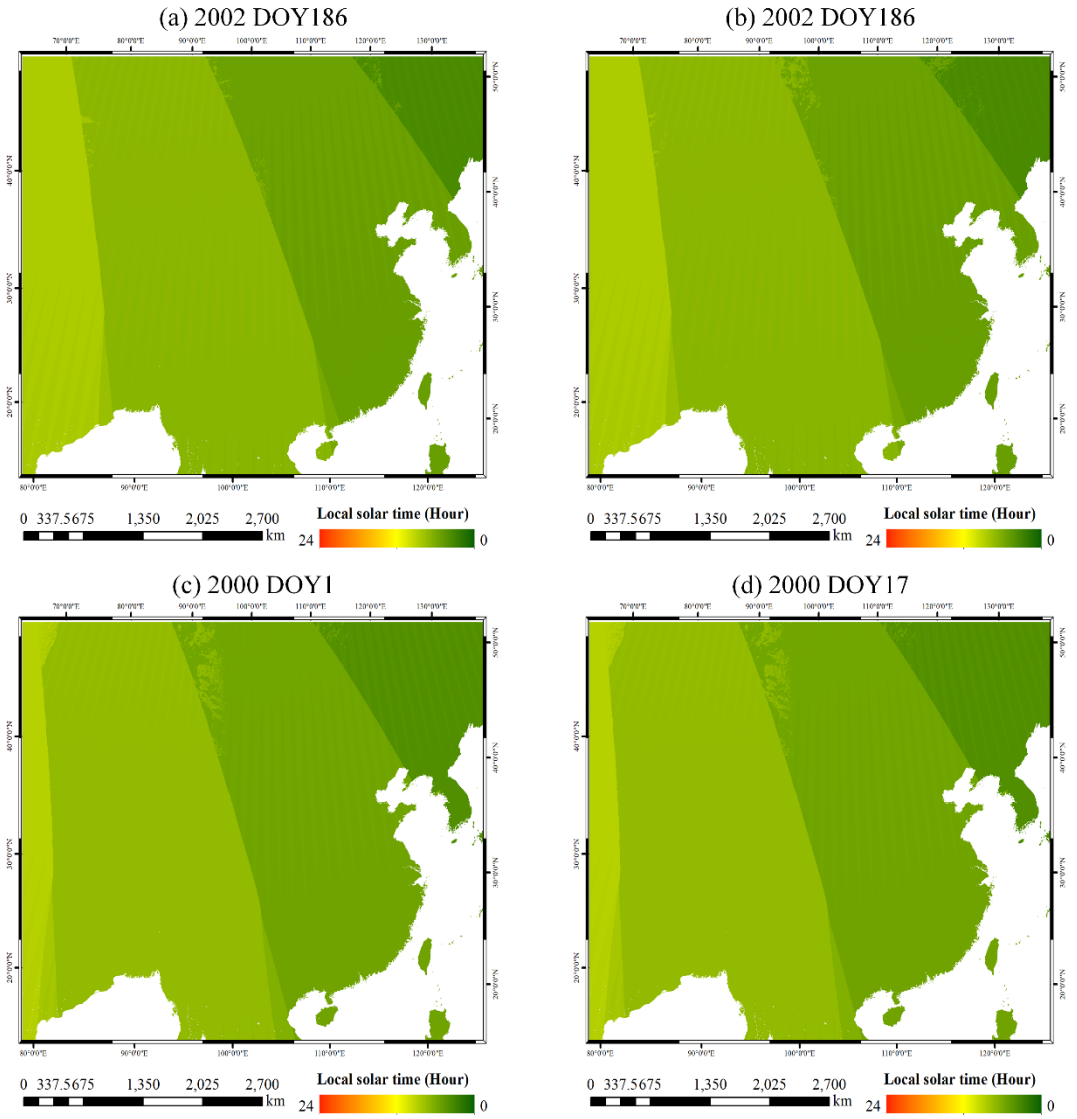


Fig.2G: Daytime Auqa overpass time on four selected days in 2000 and 2002.

**(31) Comment 31**

Line 312: clarify the interpolation method

**Authors' response:**

Thanks for your comment. We are sorry for the confusion and unclear description of interpolation. In this study, we temporally interpolated the GLDAS data and ERA5-Land with a cubic spline function based on MODIS observation time.

**(32) Comment 32**

Line 328: 'Due to limited space', all statements like this should be deleted.

**Authors' response:**

Sorry for this mistake. It has been corrected in the revised manuscript.

**(33) Comment 33**

Line 361: did the anomalies of site observations or products removed? And the grammar of the sentence is not correct.

**Authors' response:**

Sorry for this mistake. It has been corrected in the revised manuscript.

Abnormal measurements, caused by short-term disturbances such as instantaneous shadow from small clouds and birds, were excluded from the ground measured longwave radiation through a quality check. This quality check involved removing the outgoing or incoming longwave radiation that deviated by more than 3σ (standard deviations) from their respective one-hour averages (Göttsche et al., 2016). (P5, L155-158)

Reference:

Göttsche, F.-M., Olesen, F.-S., Trigo, I. F., Bork-Unkelbach, A., and Martin, M. A.: Long Term Validation of Land Surface Temperature Retrieved from MSG/SEVIRI with Continuous in-Situ Measurements in Africa, Remote Sensing, 8, 410, https://doi.org/10.3390/rs8050410, 2016.

**(34) Comment 34**

Table II: MXD11 has been suggested as having substantial bias at desert areas, and why in this table the MBE is 0.79, close to other land cover types?

**Authors' response:**

Thanks for your comment. Despite reports in the open literature of a "cold bias"

observed in desert regions of the MXD11, the MXD11A1 V6.1 product used in this paper is not significantly less accurate than the MXD21A1 in desert regions, as confirmed by validation results (Table 2D and 2E).

**(35) Comment 35**

Line 392: MXD21 has been validated that performs better than MXD11 and why it is not used?

**Authors' response:**

Thanks for your comment.

In this study, MXD11A1 was selected over MXD21A1 for the following reasons:

(i) The algorithm of the MXD11A1 V6.1 version was improved and the accuracy performance was close to that of the MXD21A1 V6.1 and better than that of the MXD11A1 V6.0. The daytime MBE of the MXD11A1 V6.1 product differed from MXD21A1 V6.1 by between -0.32 K and 2.93 K, and the RMSE differed by between -0.29 K and 1.89 K. The nighttime results are similar, with even smaller overall differences. **Note also that MODIS V6.0 data products have been decommissioned as of Monday, July 31, 2023.**

(ii) According to Yao et al. (2020), MXD11 has a stricter cloud detection treatment and fewer outliers, which is beneficial for further research and applications. The outliers were less significant in MYD11 than in MYD21 because the outliers in MYD11 were removed using temporal constraints on LST. Specifically, the extreme LSTs in MYD11 were removed using the following four steps. First, the LSTs that were higher or lower than the highest LST in 32 days by more than four times the ΔT (a variable determined by land cover) were removed. Second, the LSTs that were higher or lower than the highest LST in 16 days by more than three times the ΔT were removed. Third, the LSTs that were higher or lower than the highest LST in 8 days by more than two times the ΔT were removed. Fourth, the LSTs that were higher or lower than the 8-day average LST by more than the ΔT were removed (Wan 2008).

Table 2D: MBE, and RMSE of the daytime validation for MXD11A1, MXD11A1, and MXD21A1.

| Site | MXD11A1 V6.0 | | | | MXD11A1 V6.1 | | | | MXD21A1 V6.1 | | | |
|---|---|---|---|---|---|---|---|---|---|---|---|---|
| | MBE (K) | | RMSE (K) | | MBE (K) | | RMSE (K) | | MBE (K) | | RMSE (K) | |
| | MOD | MYD | MOD | MYD | MOD | MYD | MOD | MYD | MOD | MYD | MOD | MYD |
| DET | 2.45 | 2.01 | 5.05 | 4.65 | 1.73 | 1.88 | 4.70 | 4.70 | 2.92 | 1.56 | 5.68 | 5.39 |
| GOB | -1.23 | -2.18 | 2.69 | 3.26 | -0.61 | -1.89 | 2.25 | 2.74 | 0.52 | -1.29 | 3.66 | 3.26 |
| HZZ | 1.62 | -0.32 | 3.64 | 6.19 | 1.05 | -1.04 | 2.40 | 3.14 | 1.63 | 0.44 | 3.15 | 3.64 |
| SSW | -1.08 | -1.77 | 3.59 | 3.28 | -0.43 | -1.35 | 3.10 | 2.51 | 2.51 | 0.38 | 4.07 | 4.40 |
| GAZ | 0.12 | -1.09 | 2.44 | 3.42 | 0.47 | -0.55 | 2.37 | 2.82 | -1.30 | -2.80 | 2.07 | 3.14 |

Table 2E: MBE, and RMSE of the nighttime validation for MXD11A1, MXD11A1, and MXD21A1.

| Site | MXD11A1 V6.0 | | | | MXD11A1 V6.1 | | | | MXD21A1 V6.1 | | | |
|---|---|---|---|---|---|---|---|---|---|---|---|---|
| | MBE (K) | | RMSE (K) | | MBE (K) | | RMSE (K) | | MBE (K) | | RMSE (K) | |
| | MOD | MYD | MOD | MYD | MOD | MYD | MOD | MYD | MOD | MYD | MOD | MYD |
| DET | -0.24 | 0.18 | 1.51 | 0.88 | -0.08 | 0.16 | 0.86 | 0.97 | -0.11 | 0.24 | 2.26 | 1.87 |
| GOB | -1.53 | -1.59 | 2.13 | 1.92 | -1.62 | -1.65 | 1.96 | 1.96 | -0.58 | -0.26 | 2.71 | 1.77 |
| HZZ | 0.16 | 0.32 | 2.33 | 2.04 | -1.28 | -0.93 | 2.03 | 1.65 | 0.25 | 0.05 | 2.60 | 2.39 |
| SSW | -2.49 | -2.43 | 3.10 | 2.65 | -2.27 | -1.86 | 2.59 | 2.15 | -0.85 | -0.35 | 2.56 | 1.91 |
| GAZ | -1.55 | -0.36 | 2.34 | 1.74 | -0.68 | -0.57 | 1.90 | 1.39 | -1.50 | -0.64 | 2.83 | 2.25 |

Reference:

Wan, Z.: New refinements and validation of the collection-6 MODIS land-surface temperature/emissivity product, Remote Sensing of Environment, 140, 36–45, https://doi.org/10.1016/j.rse.2013.08.027, 2014.

Yao, R., Wang, L., Wang, S., Wang, L., Wei, J., Li, J., and Yu, D.: A detailed comparison of MYD11 and MYD21 land surface temperature products in mainland China, International Journal of Digital Earth, 1–17, https://doi.org/10.1080/17538947.2019.1711211, 2020.

**(36) Comment 36**

Sect. 4.4 Would it be better to move to the intro to clarify the importance of the data?

**Authors' response:**

Thanks for your comment. Since section 4.4 is relatively extensive, I would provide

a succinct overview of the relevant components in the introduction.

**(37) Comment 37**

Line 442: spell TPDC, please

**Authors' response:**

Thanks for your comment. It has been corrected in the revised manuscript. (P29, L584)

# Reviewer #3:

## General Comment:

Generating gap-free LST datasets have recently received increased interest. This study presented a new gap-free daily LST data set based on MODIS with unique temporal coverage (2000-2021). The manuscript was overall well written. However, additional information on data validation and comparison will better facilitate users to understand the data set and made choices.

**Authors' response:**

Thank you very much for your interest in our study and for providing valuable feedback. We greatly appreciate your reminder regarding the validation and comparison sections of the manuscript. We have carefully considered your suggestions to further improve these sections, aiming to enhance the quality of TRIMS LST and the readability of the paper. Please see our responses below. (The changes are highlighted in red in our revised manuscript.)

**(1) Comment 1**

The uniqueness of the presented data set needs to be further explained. Many gap-free LST products have been produced. The study claims that TRIMS has two additional years coverage. Datasets based on AVHRR or geostationary senor may also have coverage for 2000-2002 too. So additional justification is needed. This point is also related to the validation section. No other gap-free data were used for comparison in the current manuscript. Such comparison is very important to justify the new dataset.

**Authors' response:**

Thanks for your comment.

In recent years, various all-weather LST datasets were released (Appendix C in revised manuscript). However, all-weather LST data with both high temporal resolution (4 observations per day or higher) and high resolution (1 km or higher) since 2000 for the Chinese landmass and the surrounding areas are still rare.

As demonstrated in Appendix C, only the TRIMS LST stands out as an all-weather

LST for the period from 2000 to 2002. While AVHRR observations have coverage from 1981 to the present, the currently accessible LST products offer no spatial resolution advantage over MODIS.

Overall, the uniqueness or advantages of TRIMS LST over other datasets are in three main areas:

Firstly, the TRIMS LST in this study demonstrates comparable or better accuracy than existing publicly released all-weather/spatially seamless LST datasets. A thorough comparison with TIR LST products reveals the effectiveness of TRIMS LST, with MBD ranging from -1.5 K to 1 K and STD ranging from 1 K to 3 K, thus confirming its accuracy and consistency. Furthermore, limited in situ LST evaluations show MBE ranging from -1.64 K to 2.88 K and RMSE ranging from 1.82 K to 3.48 K. Interestingly, no significant difference is observed between clear and unclear sky conditions, indicating the robustness of TRIMS LST across various situations. Thus, based on the results of this study, TRIMS LST can be considered a reliable and accurate source of temperature data.

Second, the method employed in this study effectively overcomes the issue of boundary effects in reconstructing the all-weather process. This is achieved through the utilization of the E-RTM method, which is based on a temporal decomposition model of LST. With this model, the *LFC* and *HFC* components can be directly determined from high-resolution MODIS and ancillary remote sensing data. Consequently, only spatial downscaling of $HFC_{cld}$ is required, eliminating the need for direct downscaling of the GLDAS LST. This approach reduces the possibility of insufficient spatial downscaling. Additionally, the E-RTM method considers the relationship between LSTs of neighboring pixels, resulting in decreased errors during spatial downscaling.

Thirdly, TRIMS LST in this study offers advantages in effectively recovering LST information and preserving temporal integrity under cloudy conditions. With a spatial resolution of 1 km, TRIMS LST covers both daytime and nighttime LST from 2000 to 2022, which is comparable in spatio-temporal resolution to other published seamless LST datasets. The E-RTM method effectively recovers temperature information under clouds, ensuring clear physical meaning and high accuracy and image quality of TRIMS

LST. Moreover, TRIMS LST extends the all-weather LST data coverage of the MODIS LST time-break period of 2000-2002, providing the longest time series of its kind and enhancing the completeness of long time series LST data.

Indeed, the TRIMS LST has been widely utilized by the scientific community since its released in 2019 (Section 4.6). Other studies estimating all-weather LST have employed TRIMS LST as intercomparison data. For example, Xiao et al (2023) compared his findings with TRIMS LST and CLDAS LST, demonstrating a strong correlation between these datasets regarding their intra-annual trends (Fig.3A). Zhang et al. (2022) provided a comprehensive summary of the accuracy performance of all-weather LST products in recent years. Therefore, this study does not conduct further intercomparison with other all-weather LST products. Appendix C offers a selection of all-weather LSTs that users can choose from, based on their specific requirements such as the studied period and spatial extent.

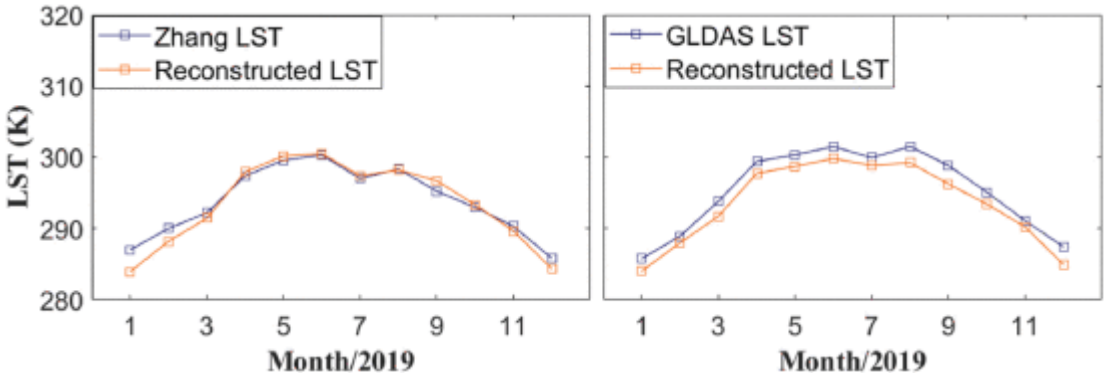


Fig.3A. Intercomparison of the reconstructed LST data with the LST product distributed by TRIMS LST (labeled as Zhang LST here) and GLDAS LST product at monthly scale (Xiao et al., 2023).

Reference:

Xiao, Y., Zhao, W., Ma, M., Yu, W., Fan, L., Huang, Y., Sun, X., and Lang, Q.: An Integrated Method for the Generation of Spatio-Temporally Continuous LST Product With MODIS/Terra Observations, IEEE Transactions on Geoscience and Remote Sensing, 61, 1–14, https://doi.org/10.1109/TGRS.2023.3254598, 2023.

Zhang, T., Zhou, Y., Zhu, Z., Li, X., and Asrar, G. R.: A global seamless 1 km resolution daily land surface temperature dataset (2003–2020), Earth Syst. Sci. Data, 14, 651–664, https://doi.org/10.5194/essd-14-651-2022, 2022.

**(2) Comment 2**

Section 4.1 compared TRIMS with two reanalysis datasets in terms of spatial patterns. In addition, TRIMS was validated against in situ in a subsequent section. Validation of the two analysis datasets using in situ should be added to provide quantitative comparison between the fused data and one of its major source data (GLDAS).

**Authors' response:**

Thanks for your comment. GLDAS LST and the ERA5-Land LST were validated against *in-situ* LST in revised manuscript.

As shown in Fig.3B, GLDAS LST is generally underestimated compared to *in-situ* LST, with MBE of -0.29 K and RMSE of 5.86 K. Under clear-sky and cloudy conditions, the GLDAS LST exhibits MBE values of 0.03 K and -0.62 K, respectively. On the other hand, ERA5-Land LST is overestimated compared to *in-situ* LST, with MBE of 1.60 K and RMSE of 6.37 K. This indicates that the accuracy of the ERA5-Land LST is lower than that of the GLDAS LST. Notably, this discrepancy is more pronounced under clear-sky conditions.

The results of the comparison with MODIS LST are shown in Fig.3C GLDAS LST is underestimated relative to MODIS LST with a small deviation, while ERA5-Land LST is overestimated relative to MODIS LST with a large deviation.

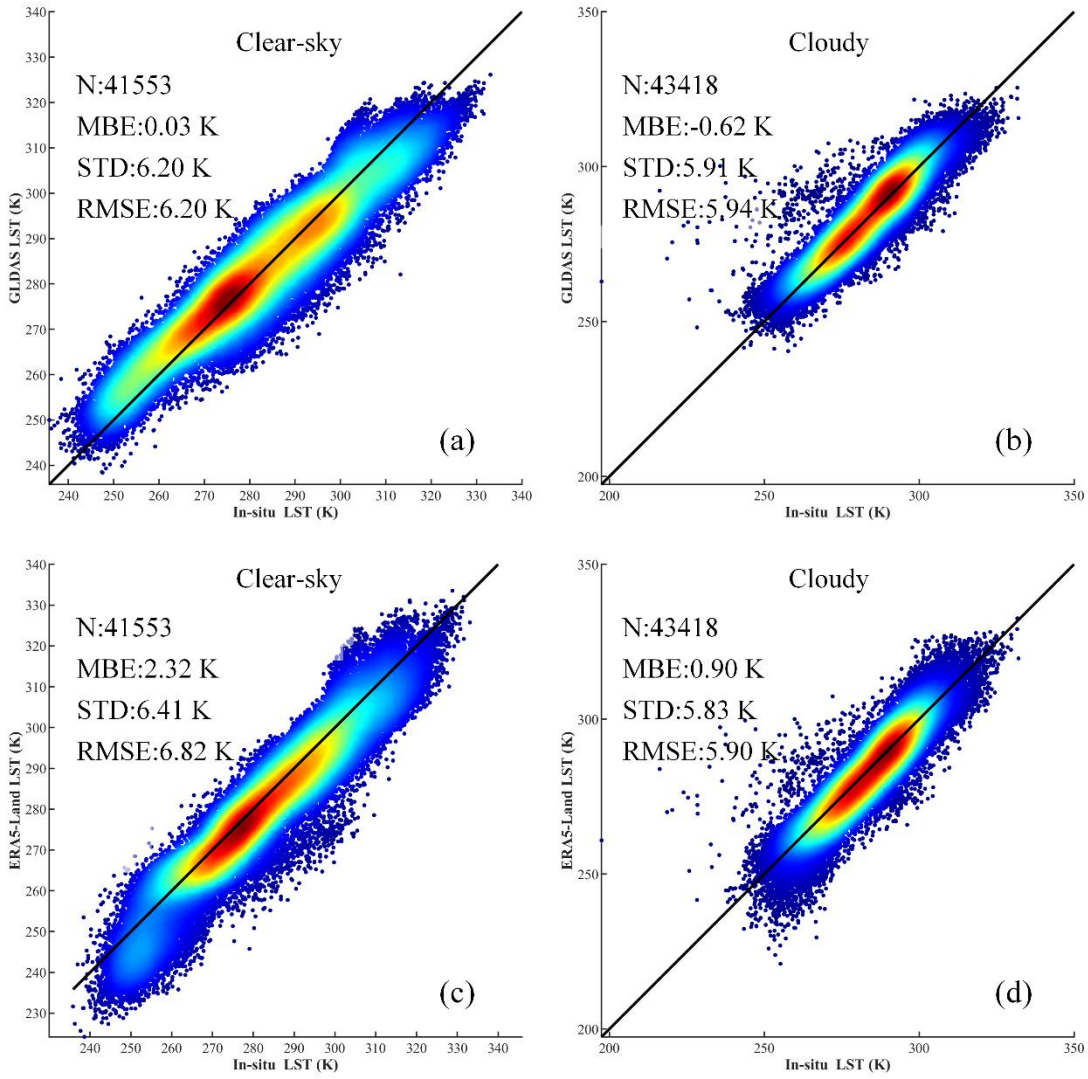


Fig.3B: Density plots between the reanalysis LST and In-situ LST.

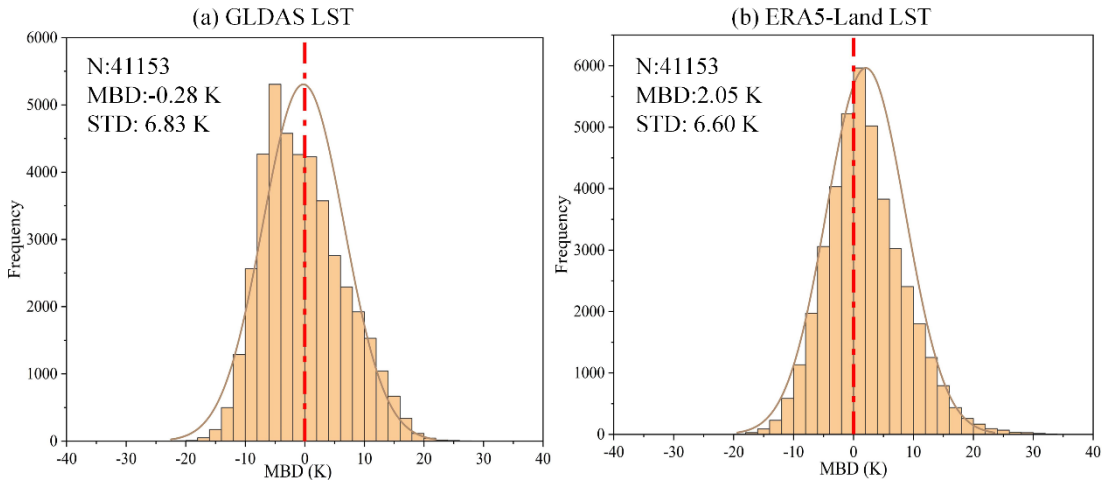


Fig.3C: Histograms of the MBD to compare reanalysis LST and MODIS LST.

Additionally, other studies have also shown the accuracy of GLDAS LST in estimating all-weather LST, with MBE ranging from -4.27 K to 8.65 K and RMSE

ranging from 3.0 K to 6.02 K (Zhang ret al.,2021; Xiao et al.,2023).

Reference:

Radakovich, J., Houser, P., Da Silva, A., and Bosilovich, M.: Results From Global Land-surface Data Assimilation Methods, AGU Spring Meeting Abstracts, 1, 2001.

Xiao, Y., Zhao, W., Ma, M., Yu, W., Fan, L., Huang, Y., Sun, X., and Lang, Q.: An Integrated Method for the Generation of Spatio-Temporally Continuous LST Product With MODIS/Terra Observations, IEEE Transactions on Geoscience and Remote Sensing, 61, 1–14, https://doi.org/10.1109/TGRS.2023.3254598, 2023.

Zhang, X., Zhou, J., Liang, S., and Wang, D.: A practical reanalysis data and thermal infrared remote sensing data merging (RTM) method for reconstruction of a 1-km all-weather land surface temperature, Remote Sensing of Environment, 260, 112437, https://doi.org/10.1016/j.rse.2021.112437, 2021.

**(3) Comment 3**

**Authors' response:**

MOD21 was reported to have superior data quality. Why did the study use MOD11 over MOD21?

**Authors' response:**

Thanks for your comment.

In this study, MXD11A1 was selected over MXD21A1 for the following reasons:

(i) The algorithm of the MXD11A1 V6.1 version was improved and the accuracy performance was close to that of the MXD21A1 V6.1 and better than that of the MXD11A1 V6.0. The daytime MBE of the MXD11A1 V6.1 product differed from MXD21A1 V6.1 by between -0.32 K and 2.93 K, and the RMSE differed by between -0.29 K and 1.89 K. The nighttime results are similar, with even smaller overall differences. Note also that MODIS V6.0 data products have been decommissioned as of Monday, July 31, 2023.

(ii) According to Yao et al. (2020), MXD11 has a stricter cloud detection treatment and fewer outliers, which is beneficial for further research and applications. The outliers were less significant in MYD11 than in MYD21 because the outliers in MYD11 were removed using temporal constraints on LST. Specifically, the extreme LSTs in MYD11 were removed using the following four steps. First, the LSTs that were higher or lower than the highest LST in 32 days by more than four times the ΔT (a variable determined by land cover) were removed. Second, the LSTs that were higher or lower than the highest LST in 16 days by more than three times the ΔT were removed. Third, the LSTs that were higher or lower than the highest LST in 8 days by more than two times the ΔT were removed. Fourth, the LSTs that were higher or lower than the 8-day average LST by more than the ΔT were removed (Wan 2008).

Table 3A: MBE, and RMSE of the daytime validation for MXD11A1, MXD11A1 and MXD21A1.

| Site | MXD11A1 V6.0 | | | | MXD11A1 V6.1 | | | | MXD21A1 V6.1 | | | |
|---|---|---|---|---|---|---|---|---|---|---|---|---|
| | MBE (K) | | RMSE (K) | | MBE (K) | | RMSE (K) | | MBE (K) | | RMSE (K) | |
| | MOD | MYD | MOD | MYD | MOD | MYD | MOD | MYD | MOD | MYD | MOD | MYD |
| DET | 2.45 | 2.01 | 5.05 | 4.65 | 1.73 | 1.88 | 4.70 | 4.70 | 2.92 | 1.56 | 5.68 | 5.39 |
| GOB | -1.23 | -2.18 | 2.69 | 3.26 | -0.61 | -1.89 | 2.25 | 2.74 | 0.52 | -1.29 | 3.66 | 3.26 |
| HZZ | 1.62 | -0.32 | 3.64 | 6.19 | 1.05 | -1.04 | 2.40 | 3.14 | 1.63 | 0.44 | 3.15 | 3.64 |
| SSW | -1.08 | -1.77 | 3.59 | 3.28 | -0.43 | -1.35 | 3.10 | 2.51 | 2.51 | 0.38 | 4.07 | 4.40 |
| GAZ | 0.12 | -1.09 | 2.44 | 3.42 | 0.47 | -0.55 | 2.37 | 2.82 | -1.30 | -2.80 | 2.07 | 3.14 |

Table 3B: MBE, and RMSE of the nighttime validation for MXD11A1, MXD11A1 and MXD21A1.

| Site | MXD11A1 V6.0 | | | | MXD11A1 V6.1 | | | | MXD21A1 V6.1 | | | |
|---|---|---|---|---|---|---|---|---|---|---|---|---|
| | MBE (K) | | RMSE (K) | | MBE (K) | | RMSE (K) | | MBE (K) | | RMSE (K) | |
| | MOD | MYD | MOD | MYD | MOD | MYD | MOD | MYD | MOD | MYD | MOD | MYD |
| DET | -0.24 | 0.18 | 1.51 | 0.88 | -0.08 | 0.16 | 0.86 | 0.97 | -0.11 | 0.24 | 2.26 | 1.87 |
| GOB | -1.53 | -1.59 | 2.13 | 1.92 | -1.62 | -1.65 | 1.96 | 1.96 | -0.58 | -0.26 | 2.71 | 1.77 |
| HZZ | 0.16 | 0.32 | 2.33 | 2.04 | -1.28 | -0.93 | 2.03 | 1.65 | 0.25 | 0.05 | 2.60 | 2.39 |
| SSW | -2.49 | -2.43 | 3.10 | 2.65 | -2.27 | -1.86 | 2.59 | 2.15 | -0.85 | -0.35 | 2.56 | 1.91 |
| GAZ | -1.55 | -0.36 | 2.34 | 1.74 | -0.68 | -0.57 | 1.90 | 1.39 | -1.50 | -0.64 | 2.83 | 2.25 |

Reference:

Wan, Z.: New refinements and validation of the collection-6 MODIS land-surface temperature/emissivity product, Remote Sensing of Environment, 140, 36–45, https://doi.org/10.1016/j.rse.2013.08.027, 2014.

Yao, R., Wang, L., Wang, S., Wang, L., Wei, J., Li, J., and Yu, D.: A detailed comparison of MYD11 and MYD21 land surface temperature products in mainland China, International Journal of Digital Earth, 1–17, https://doi.org/10.1080/17538947.2019.1711211, 2020.

**(4) Comment 4**

Do the authors have the plan to extend the dataset to global coverage?

**Authors' response:**

Thanks for your comment.

In this study, it is important to acknowledge that the E-RTM method used does not offer advantages in terms of computational time. This is due to the complex parameterisation process involving multiple sources of data and pixel-by-pixel. Consequently, obtaining a global, all-weather LST over the past 20-40 years and avoiding LST discrepancies caused by cloud cover has proven to be challenging (Long et al., 2020; Zhang et al., 2021; Zhang et al., 2022). In order to address these challenges, future work will require a combination of high-quality data and robust and efficient algorithms to produce global all-weather LST data.

Reference:

Long, D., Yan, L., Bai, L., Zhang, C., Li, X., Lei, H., Yang, H., Tian, F., Zeng, C., Meng, X., and Shi, C.: Generation of MODIS-like land surface temperatures under all-weather conditions based on a data fusion approach, Remote Sensing of Environment, 246, 111863, https://doi.org/10.1016/j.rse.2020.111863, 2020.

Zhang, X., Zhou, J., Liang, S., and Wang, D.: A practical reanalysis data and thermal infrared remote sensing data merging (RTM) method for reconstruction of a 1-km all-weather land surface temperature, Remote Sensing of Environment, 260, 112437, https://doi.org/10.1016/j.rse.2021.112437, 2021.

Zhang, T., Zhou, Y., Zhu, Z., Li, X., and Asrar, G. R.: A global seamless 1 km resolution daily land surface temperature dataset (2003–2020), Earth Syst. Sci. Data, 14, 651–664, https://doi.org/10.5194/essd-14-651-2022, 2022.